JETIR.ORG ISSN: 2349-5162 | ESTD Year : 2014 | Monthly Issue
JOURNAL OF EMERGING TECHNOLOGIES AND INNOVATIVE RESEARCH (JETIR)
An International Scholarly Open Access, Peer-reviewed, Refereed Journal

SYNTHESIS OF NEEM BARK-BASED NANOADSORBENT FOR EFFICIENT TOLUIDINE DYE REMOVAL: A COMPREHENSIVE KINETIC, ISOTHERM, AND THERMODYNAMIC INVESTIGATION

[1]Rekha Sharma, [2]Bhanupriya Mordhiya, [3]Pooja Meena, [4]Ashish Dev Kanwadia, [5]Pooja
[1]Research Scholar, [2]Asistant Professor, [3]Research Scholar, [4]Research Scholar, [5]Research Scholar
[1,2,3,4,5]Department of Chemistry, University of Rajasthan, Jaipur (Rajasthan) INDIA

Abstract: In this study, the adsorption behavior of the cationic organic dye Toluidine Blue (TB) from aqueous solution was explored using a nanoadsorbent derived from the dead bark of *Azadirachta indica* (neem). The synthesized activated carbon was characterized using FTIR, zeta potential analysis, UV-Vis spectroscopy, FESEM, BET, and TEM techniques. The N_2 adsorption–desorption analysis revealed a type IV isotherm with an H3 hysteresis loop, indicating the formation of mesoporous structures with pore diameters ranging from 2–50 nm. Batch adsorption experiments were conducted to evaluate equilibrium isotherms, investigating the influence of key parameters such as contact time, pH, temperature, initial dye concentration, and adsorbent dosage. Under optimized conditions, 20 mg/L initial dye concentration, pH 12, and 20 mg adsorbent dose, a maximum removal efficiency of 98.76% was achieved within 70 minutes. However, at higher initial dye concentrations (60 mg/L), the removal efficiency decreased to 82.28% under similar conditions.

The adsorption data aligned well with the Langmuir isotherm model, as evidenced by a high correlation coefficient ($R^2 = 0.999$), and the maximum adsorption capacity was estimated to be 106.92 mg/g at 303 K. Kinetic analysis confirmed that the adsorption followed a pseudo-second-order model, and although intra-particle diffusion contributed to the process, it was not the sole rate-limiting step. Thermodynamic parameters indicated the spontaneous and endothermic nature of the adsorption, with negative $\Delta G°$, positive $\Delta H°$, and positive $\Delta S°$, suggesting increased randomness at the solid–liquid interface during dye uptake.

Keywords: *Azadirachta indica*, Toluidine Blue, Adsorption, Zeta Potential, Isotherm, Kinetics, Thermodynamics.

I. INTRODUCTION

The rapid growth in dye production and its widespread application across multiple industries such as textiles, food processing, pharmaceuticals, dyeing, paper, and leather has significantly contributed to environmental pollution in recent decades [1–3]. Among various pollutants, synthetic dyes are particularly concerning due to their complex molecular structures, resistance to degradation, and toxic nature. When discharged into water bodies without proper treatment, dye-laden effluents impart intense coloration to water, which disrupts the aquatic ecosystem by inhibiting sunlight penetration [4-8]. This, in turn, hampers photosynthetic activity and leads to reduced oxygen levels, affecting aquatic flora and fauna. Beyond environmental concerns, many dyes are known to exhibit toxicological effects on human health. Exposure to these dyes, whether through contaminated water or occupational contact, has been associated with allergic dermatitis, skin irritation, mutagenic changes, and even carcinogenic outcomes [9-10]. Given these profound implications, it becomes imperative to treat dye-contaminated wastewater before its discharge into the natural environment. Effective removal of dyes not only mitigates health and ecological risks but also ensures compliance with environmental safety regulations. To address the issue of dye contamination in water, several treatment methods have been explored, such as adsorption, diffusion, membrane filtration (including ultrafiltration), coagulation, chemical and electrochemical oxidation, reverse osmosis, and biological approaches involving aerobic and anaerobic microbial degradation [11-14]. Adsorption is a highly effective technique for dye removal due to its simplicity, cost-efficiency, and ability to remove a wide range of dyes even at low concentrations. It offers high removal efficiency, minimal sludge generation, and suitability for regeneration and reuse of adsorbents, making it an eco-friendly solution for wastewater treatment [15-17]. Agricultural and plant residues such as rice husk, sawdust, banana peel, coconut shell, neem bark, and sugarcane bagasse have been widely utilized as low-cost, eco-friendly adsorbents for dye removal. These lignocellulosic materials possess abundant functional groups and porous structures, enhancing their adsorption capacity for various

synthetic dyes [18-22]. Toluidine Blue (TB) is a phenothiazine-based dye that has found extensive applications across multiple fields, including medical sciences, the textile industry, and biotechnology [23-24]. It serves numerous functions, such as acting as a mediator in chemical and biochemical reactions, a colorant for fabrics, a photosensitizer in studies involving photoactivated microorganisms, and a labeling agent for microbial identification [25-27].

This study aims to explore an efficient and cost-effective method for the removal of Toluidine Blue, a water-soluble dye, from aqueous solutions through adsorption using a nanoadsorbent prepared from the dead bark of *Azadirachta indica* (neem). The research focuses on evaluating the effects of key parameters such as initial dye concentration, solution pH, contact time, and temperature on the adsorption performance. Additionally, the adsorption kinetics, isotherm, thermodynamics, and underlying mechanism of Toluidine Blue dye removal have been thoroughly investigated.

II. Materials and Methods

A. Chemical Used

The present study employed the following chemicals: phosphoric acid (H_3PO_4), hydrochloric acid (HCl), sodium hydroxide (NaOH), distilled water, methylene blue dye, and naturally dried dead bark of *Azadirachta indica* (neem). All chemicals were of analytical grade and were used without further purification. A stock solution of Toluidine Blue (TB) was prepared by dissolving 1.0 g of dye per liter in double-distilled water.

Toluidine Blue was selected as a representative cationic organic dye for evaluating the adsorption performance of the prepared nanoadsorbent. TB is a synthetic, heterocyclic, water-soluble basic dye with the molecular formula $C_{15}H_{16}N_3S^+$ and a molecular weight of 270.374 $g \cdot mol^{-1}$. It exhibits high stability in aqueous media under ambient conditions. However, due to its toxic, carcinogenic, and non-biodegradable nature, Toluidine Blue is considered a hazardous pollutant and poses significant risks to aquatic ecosystems and human health [28-30]. The chemical structure of Toluidine Blue is presented in Figure 1.

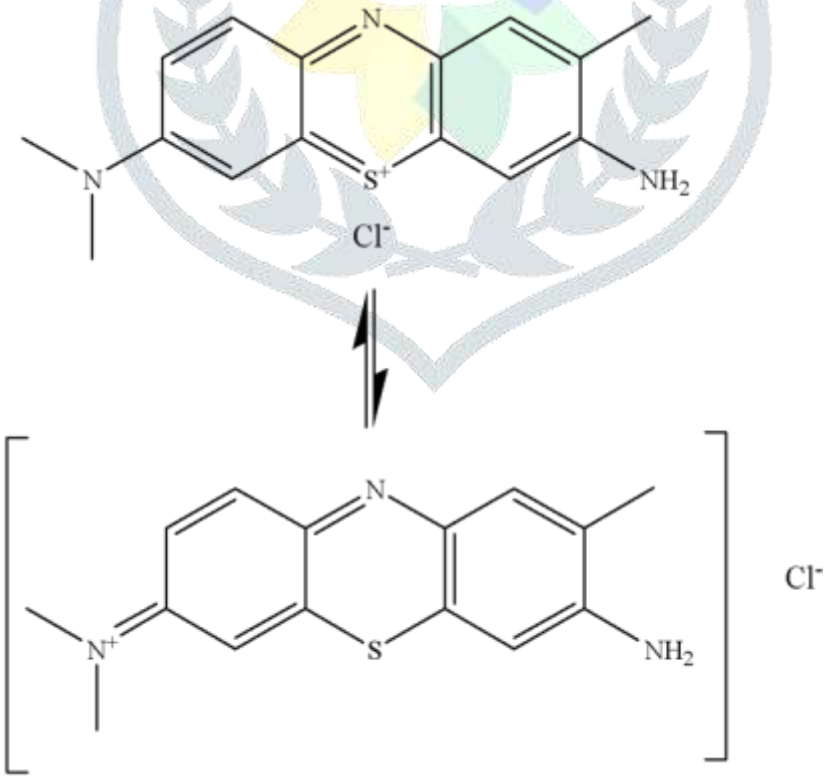

Figure 1: Toluidine blue (TB) dye structure

B. Fabrication of Nanostructured Adsorbent

i. Pyrolytic Conversion of Dead Azadirachta indica Bark

The naturally desiccated and senescent bark of the *Azadirachta indica* (neem) plant was systematically collected from the university campus. Initially, the bark was manually segmented into smaller fragments and subjected to repetitive washing with tap water to remove adhering particulates and surface impurities. This was followed by thorough rinsing with distilled water to eliminate any residual contaminants. The cleaned bark samples were subsequently oven-dried at 80°C for 24 hours to ensure complete moisture removal and material stabilization. Post-drying, the biomass was transferred to a ceramic crucible, covered with aluminium foil to maintain a low-oxygen environment, and thermally treated at 400°C for 2 hours in a muffle furnace to induce carbonization. Upon gradual cooling to ambient temperature, the resulting carbonized black residue was finely pulverized using a mortar and pestle to obtain a uniform activated carbon nanoadsorbent, suitable for adsorption studies.

ii. Impregnation and Activation with Phosphoric Acid

A chemical activation procedure was employed to enhance the adsorptive properties of the neem bark-derived charcoal. In the standard method, 1 g of pre-carbonized neem charcoal was impregnated with 5 mL of concentrated phosphoric acid (H_3PO_4), and the

mixture was allowed to stand overnight to facilitate thorough penetration and surface modification. Subsequently, the impregnated material was oven-dried at 90 °C for 5 hours to remove excess acid and moisture. The partially dried mass was then subjected to secondary thermal treatment in a muffle furnace at 500 °C for 2 hours, promoting further activation and structural development of the carbon matrix. Following carbonization, the activated product was allowed to cool to room temperature and was repeatedly washed with distilled water to remove residual acid content. A final wash with ethyl alcohol was performed to enhance surface purity. The sample was then oven-dried at 85 °C for 3 hours to yield the final nanoadsorbent of activated carbon from neem bark. The resulting nanoadsorbent was subsequently utilized for the removal of dye from aqueous solutions under varying pH conditions.

C. Characterization Techniques and Instrumentation

To comprehensively evaluate the surface morphology, textural properties, microstructure, chemical composition, crystallinity, bonding characteristics, and functional groups of the synthesized nanoadsorbent, a series of advanced analytical techniques was employed. The identification of surface functional groups and chemical bonds was performed using Fourier Transform Infrared (FTIR) Spectroscopy in transmission mode within the range of 4000–400 cm^{-1}, utilizing a Perkin Elmer FTIR spectrometer. The microstructural and surface morphological features of the developed adsorbent were examined through Field Emission Scanning Electron Microscopy (FESEM) using a Nova Nano FESEM-450 (FEI), and Transmission Electron Microscopy (TEM) was conducted using an FEI CM12 instrument for deeper insight into the nanostructure. The textural characteristics, including specific surface area, pore volume, and pore size distribution, were analyzed using the Brunauer-Emmett-Teller (BET) method with a NOVAtouch 2LX surface area and porosity analyzer. Quantification of the residual concentration of TB dye in aqueous solutions after adsorption was carried out using a UV–Visible spectrophotometer (Shimadzu UV-2600) by measuring the absorbance at $\lambda = 627$ nm.

D. Dye Adsorption Experiments under Batch Conditions

To assess the dye removal efficiency of the synthesized nanoadsorbent, batch adsorption experiments were conducted using aqueous solutions of TB dye. The effects of several operational parameters, including adsorbent dosage, solution pH, temperature, initial dye concentration, and contact time, were systematically examined. Working solutions of varying concentrations were prepared by diluting the stock TB dye solution. In each experiment, 50 mL of TB dye solution was placed in a 250 mL Erlenmeyer flask and agitated on a thermostatic orbital shaker under optimized conditions at room temperature. The experimental ranges were as follows: initial dye concentration varied from 20 to 70 mg/L, adsorbent dosage from 20 to 40 mg, contact time from 10 to 80 minutes, and solution pH ranged from 4 to 12. The pH of the dye solution was adjusted using 0.1 M NaOH or 0.1 M HCl.

At predetermined time intervals, the remaining concentration of TB dye in the solution was determined by measuring the absorbance at 627 nm using a UV–Visible spectrophotometer. The data obtained were used to calculate the equilibrium adsorption capacity (q_e), the instantaneous adsorption capacity (q_t), and the percentage removal efficiency of TB dye.

$$q_e = \left(\frac{C_o - C_e}{m}\right) \times V \qquad (1)$$

$$\%\,Removal = \left(\frac{C_o - C_e}{m}\right) \times 100 \qquad (2)$$

$$q_t = \left(\frac{C_O - C_t}{m}\right) \times V \qquad (3)$$

Where V represents the volume of the dye solution in liters (L), m denotes the mass of the adsorbent in grams (g). C_o, C_t, and C_e (all in mg/L) correspond to the initial dye concentration, the concentration at time t, and the equilibrium concentration of TB dye, respectively [31-33].

III. Results and Discussions

A. Structural Analysis of the Synthesized Nanoadsorbent

The prepared AC-MO nanoadsorbent has been characterized using the following methods

i. FTIR Spectral Interpretation

The FTIR spectrum of the synthesized activated carbon-based nanoadsorbent reveals several distinct absorption bands, indicating the presence of various functional groups on its surface. A broad band observed in the region of 3400–3600 cm^{-1} corresponds to O–H stretching vibrations, suggesting the presence of hydroxyl groups from adsorbed moisture or surface-bound alcohols and phenols. Peaks in the range of 2920–2850 cm^{-1} are attributed to C–H stretching vibrations of aliphatic $–CH_2$ and $–CH_3$ groups, likely arising from residual organic matter. A strong peak around 1700–1600 cm^{-1} is associated with C=O stretching vibrations, indicating carbonyl-containing groups such as carboxylic acids, ketones, or aldehydes. The band appearing near 1400–1450 cm^{-1} corresponds to C–H bending or C–C skeletal vibrations, suggesting the presence of aromatic ring structures. A sharp absorption peak in the range of 1100–1000 cm^{-1} is linked to C–O stretching vibrations, indicative of alcohols, ethers, or esters. Additionally, the region below 900 cm^{-1} exhibits bands related to out-of-plane bending vibrations of aromatic C–H bonds, further supporting the existence of aromatic functionalities in the carbon matrix. Collectively, these spectral features confirm the presence of oxygen-containing functional groups (–OH, –COOH, –C=O, –C–O) on the surface of the nanoadsorbent, which enhance its surface polarity and facilitate effective adsorption of cationic dyes such as Toluidine Blue through mechanisms involving electrostatic interactions and hydrogen bonding.

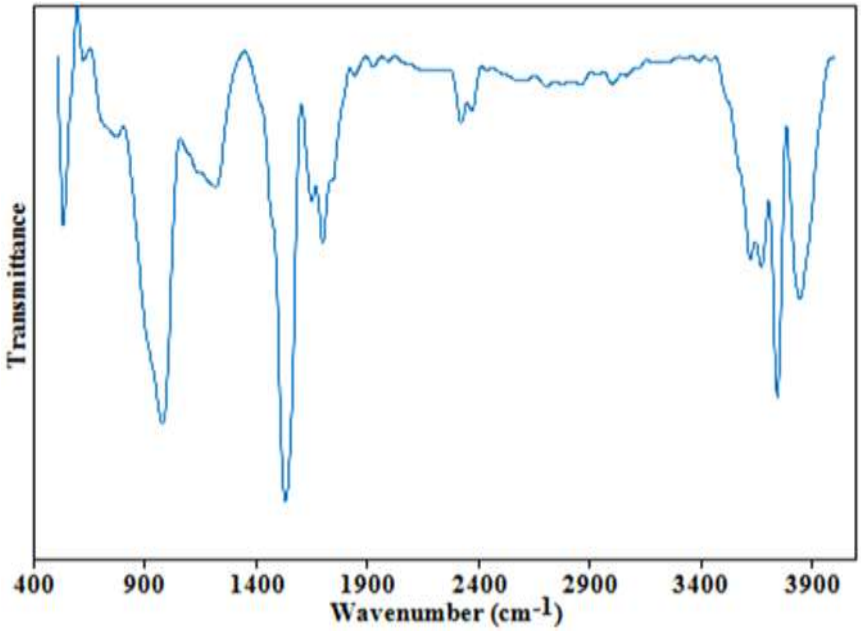

Figure 2: FTIR analysis of prepared nanoadsorbent of *Azadirachta indica*

ii. Surface Morphology Study Using FESEM

The synthesized nanoadsorbent was subjected to morphological characterization using Scanning Electron Microscopy (SEM), as shown in Figure 3 (a–f) at different magnifications. The SEM images reveal a rough, blistered surface with a porous, sheet-like architecture. This morphology consists of numerous open pores and interconnected hollow chambers, indicating a well-developed porous network. Such structural features enhance the surface area and adsorption capability of the neem-based activated carbon, making it a promising candidate for the effective removal of contaminants from aqueous solutions.

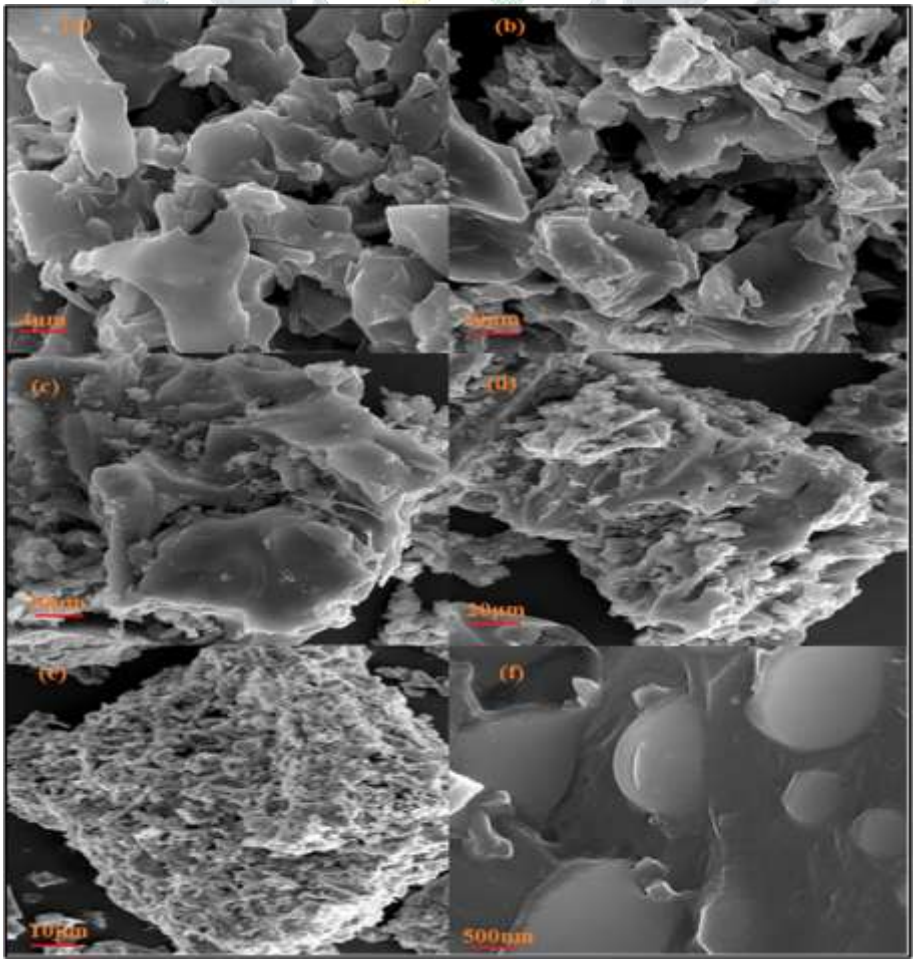

Figure 3: Surface morphology of neem-based nanoadsorbent observed through FESEM analysis.

iii. Nanostructural Analysis by HRTEM

Transmission Electron Microscopy (TEM) analysis, presented in Figure 4 (a–f), illustrates the topological features of the neem bark-derived activated carbon. The images reveal an uneven and porous texture, characteristic of effective adsorbent materials. Furthermore, the Selected Area Electron Diffraction (SAED) pattern in Figure 4(f) displays a diffused bright ring, indicating the amorphous or poorly crystalline nature of the material [34]. This combination of high porosity and surface roughness contributes to an enhanced surface area, thereby facilitating the efficient adsorption of dye molecules.

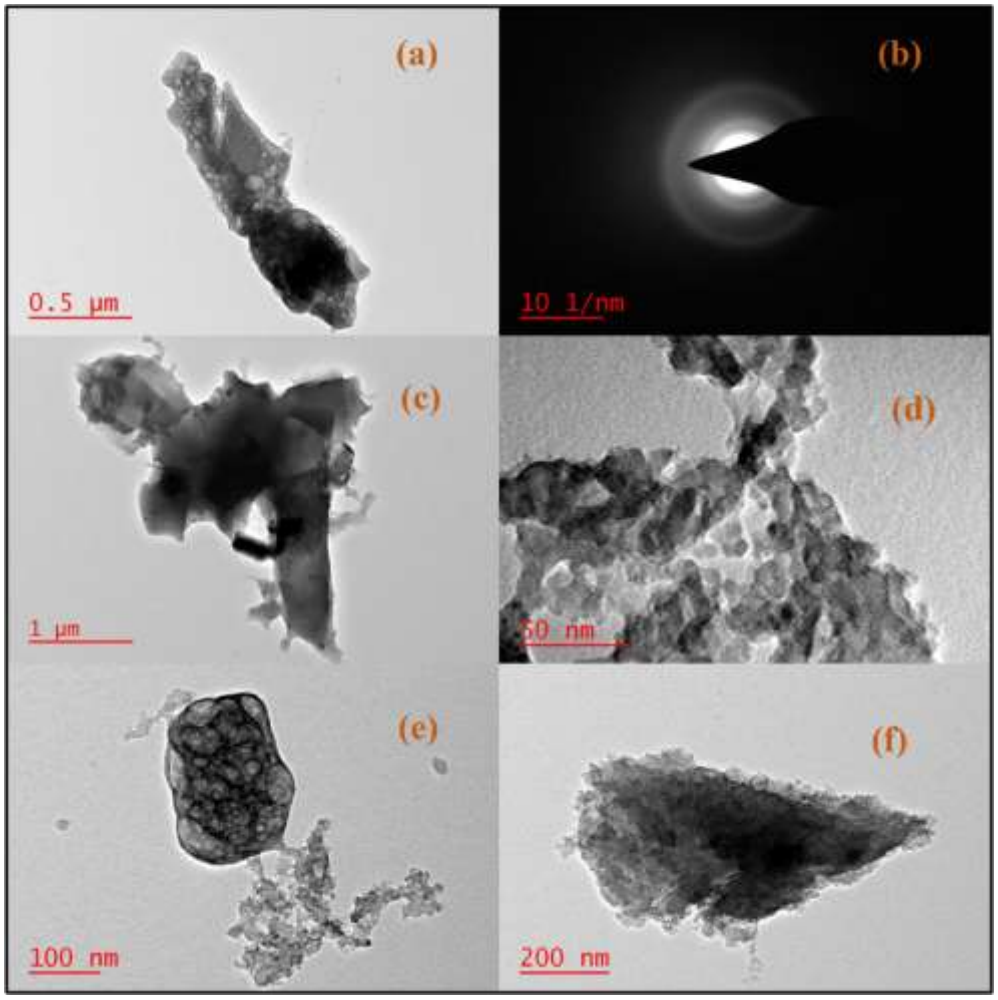

Figure 4: Nanostructural analysis of neem bark-derived activated carbon using HRTEM.

iv. Surface Charge Characterization via Zeta Potential

The zeta potential analysis of the synthesized nanoadsorbent (Figure 5) reveals a negative surface charge with a peak value around –26.5 mV. This moderately negative zeta potential suggests that the particles possess sufficient electrostatic repulsion to remain dispersed, thus maintaining colloidal stability in aqueous media. A negative surface charge also enhances the adsorptive interaction with cationic dye molecules, contributing to efficient dye removal from aqueous media.

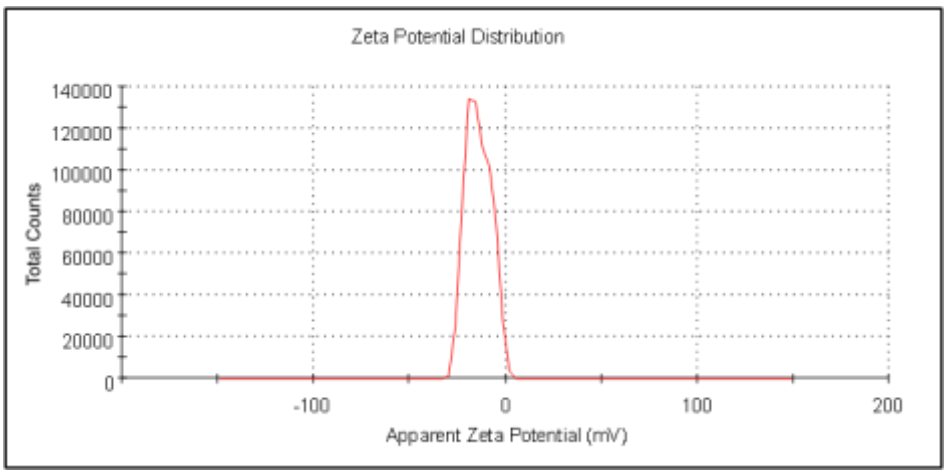

Figure 5: Zeta potential distribution of neem bark-derived nanoadsorbent

v. Surface Area and Pore Structure Analysis (BET)

The neem bark-based activated carbon nanoadsorbent was characterized using BET analysis to determine its surface area, total pore volume, and pore size distribution (PSD). As illustrated in Figure 6(a), the N_2 adsorption–desorption isotherm follows a Type IV pattern with an H3 hysteresis loop, in line with IUPAC guidelines, signifying the mesoporous character of the material [35]. The noticeable increase in nitrogen uptake at elevated relative pressure (P/P_0) reflects the presence of well-developed mesopores. Figure 6(b) presents the multipoint BET plot of the sample, confirming the porous structure. The BJH analysis in Fig. 6(c) reveals that most pores fall within the 3–20 nm range, with a dominant pore size around 3 nm. Additionally, the DFT-based PSD analysis (Fig. 6(d)) indicates an average pore diameter of nearly 3 nm, supporting the mesoporous architecture of the synthesized carbon adsorbent [36]. The presence of such fine mesopores enhances the surface area and facilitates efficient adsorption of dye molecules.

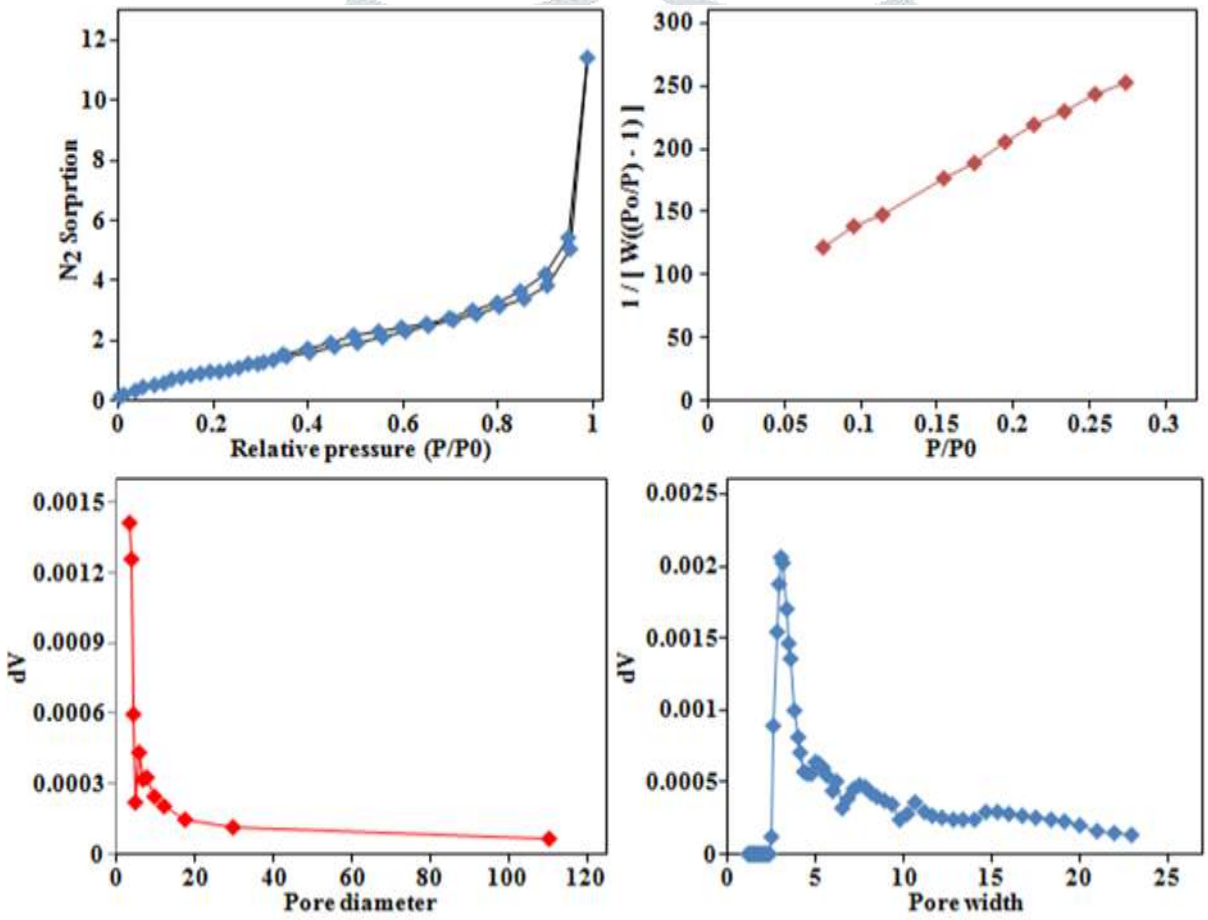

Figure 6: (a) Nitrogen adsorption–desorption isotherm, (b) BET surface area analysis, and (c, d) BJH pore size distribution curves of activated carbon derived from *Azadirachta indica* (neem) bark.

B. Experimental Variables in Adsorption Studies

i. Time-Dependent Adsorption Behavior

The effectiveness of the synthesized nanoadsorbent in removing TB dye was assessed by varying the contact time from 10 to 80 minutes, as illustrated in Figure 7. Initially, the adsorption rate increased sharply with time and reached equilibrium at around 70 minutes. Beyond this point, the adsorption and desorption rates stabilized, indicating that equilibrium had been established. Therefore, 70 minutes was identified as the optimal contact time for maximum dye removal. The rapid uptake at the beginning is attributed to the high concentration of dye and the abundance of active sites available on the adsorbent surface. As the contact time increases, these sites become progressively occupied, resulting in a gradual decline in adsorption rate. Once equilibrium is reached, no significant improvement in dye removal was observed, even with extended contact time up to 80 minutes, due to the saturation of adsorption sites on the nanoadsorbent surface [37].

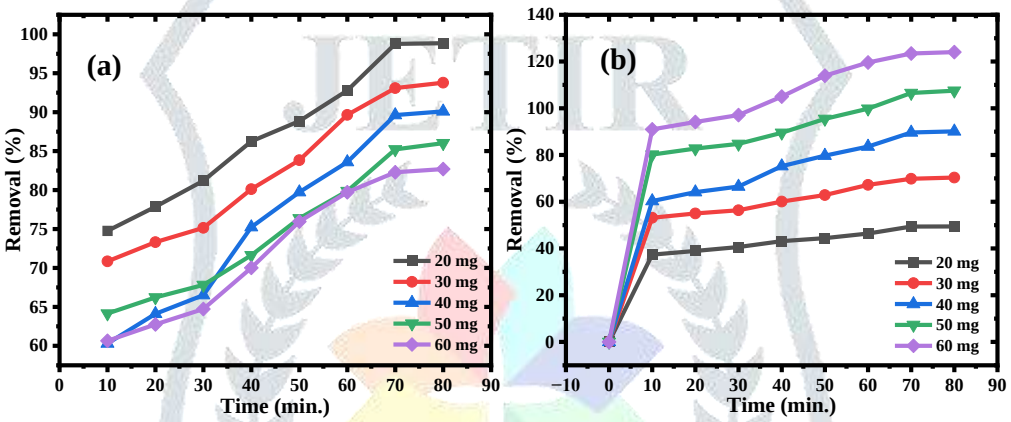

Figure 7: Effect of varying contact time on the adsorption efficiency of TB dye using neem bark-derived activated carbon nanoadsorbent.

ii. Effect of pH on Dye Removal Performance

To evaluate the influence of pH on the adsorption efficiency of Toluidine Blue (TB) dye, the solution pH was varied from 4 to 12, as shown in Fig. 8(a). The experimental results demonstrate a significant enhancement in dye removal efficiency with increasing pH. The adsorption performance of the synthesized nanoadsorbent improved from 72.12% at lower pH to a maximum of 98.33% at higher pH, indicating that alkaline conditions favor the adsorption of the cationic dye onto the adsorbent surface.

iii. Impact of Initial Dye Concentration on Adsorption Capacity

The influence of initial TB dye concentration on its adsorption by neem bark-derived activated carbon nanoadsorbent was assessed by varying the concentration from 20 to 70 mg/L, using an optimized adsorbent dose of 20 mg and pH 12, as shown in Fig. 8(b). A decrease in removal efficiency from 98.63 % to 63.89 % was observed with increasing dye concentration, while the adsorption capacity (qt) increased from 16.43 to 63.89 mg/g within 80 minutes of contact time [Fig. 8(b)]. Consequently, 20 mg/L was selected as the working concentration for isotherm and thermodynamic evaluations. The higher removal efficiency at lower concentrations can be attributed to the greater availability of vacant adsorption sites. In contrast, at elevated concentrations, the saturation of active sites by excess dye molecules leads to a decline in removal percentage [38]. Thus, at higher initial concentrations, the adsorptive efficiency of the neem bark-based carbon decreases due to site occupancy limitations.

iv. Impact of Adsorbent Amount on Adsorption Capacity

Fig. 8 (c) illustrates the influence of varying adsorbent dosages on the removal efficiency of TB dye. As the dosage was increased from 20 mg to 40 mg, the dye removal efficiency improved markedly from 81.18 % to 98.60%. However, beyond 40 mg, the adsorption capacity plateaued, suggesting no significant enhancement in performance. Consequently, a dosage of 20 mg was selected for further investigations. The observed improvement in dye removal with increased adsorbent mass is likely due to the greater number of active sites and expanded surface area available for adsorption under fixed dye concentration and solution volume conditions [39].

v. Influence of Temperature on Adsorption Process

An increase in the temperature of the TB dye solution up to 45 °C led to a slight enhancement in the adsorption efficiency of neem bark-derived activated carbon nanoadsorbent, improving from 98.19% to 98.97%, as presented in Figure 8(d). Correspondingly, the equilibrium adsorption capacity rose from 49.09 mg g^{-1} to 49.48 mg g^{-1}. This improvement may be attributed to reduced solution viscosity at elevated temperatures, which facilitates faster dye diffusion. Additionally, the increased intra-particle diffusion of dye molecules at higher temperatures further contributes to enhanced adsorption. These observations support the endothermic nature of the adsorption process, as the uptake improves with temperature rise [40].

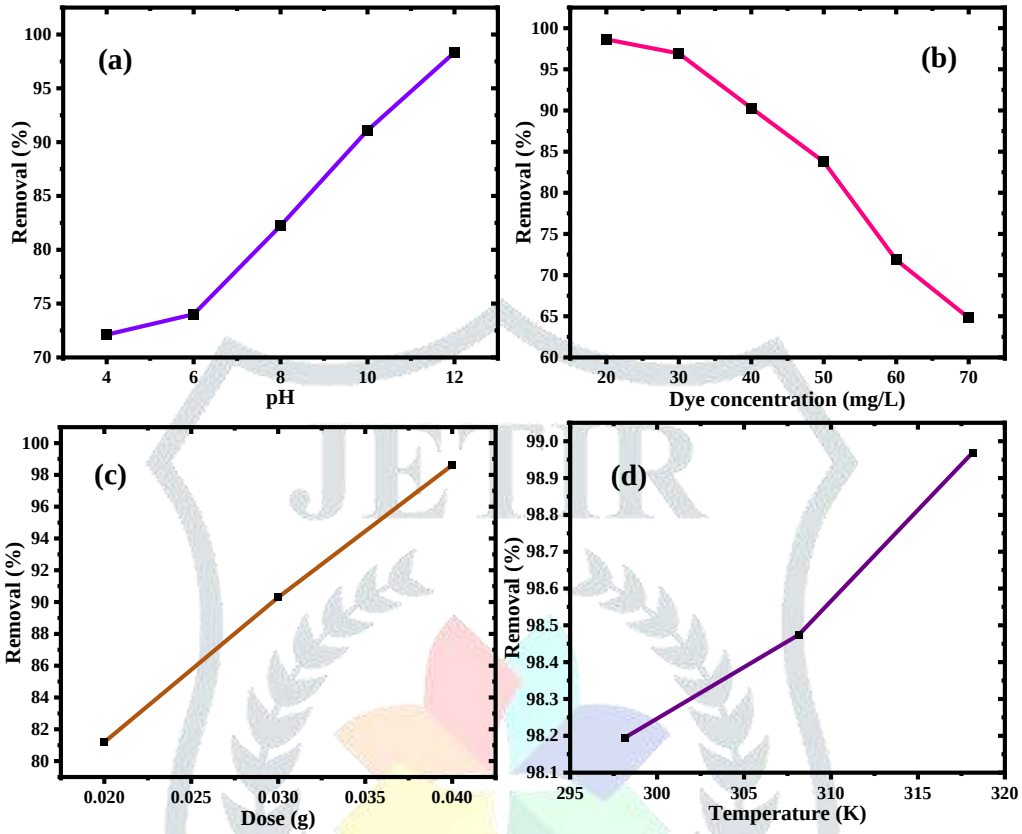

Figure 8: Influence of (a) solution pH, (b) dye concentration, (c) adsorbent dose, and (d) temperature on the adsorption performance of nanoadsorbent derived from neem bark.

C. Kinetics study of adsorption

The adsorption behavior of TB dye on the synthesized nanoadsorbent of activated carbon of neem bark was analyzed through kinetic modeling to understand the underlying mechanism and rate-controlling steps better. Commonly used models, pseudo-first-order (PFO), pseudo-second-order (PSO), Elovich, and intra-particle diffusion (IPD), were applied to fit the experimental data across various initial concentrations (20–70 mg/L), as summarized in Table 1. At the same time, their corresponding kinetic plots are presented in Figure 9. Among the applied models, the PSO model exhibited the best correlation, as evidenced by higher R^2 values and the close alignment between experimental ($q_{e,exp}$) and calculated ($q_{e,cal}$) adsorption capacities. This suggests that the adsorption of TB onto the nanoadsorbent's surface predominantly follows a chemisorption mechanism, involving electron exchange or sharing between dye molecules and functional groups on the adsorbent. In contrast, the PFO model yielded lower R^2 values and showed greater deviation between predicted and observed q_e values, indicating a weaker fit.

Additionally, a decreasing trend in the PSO rate constant (K_2) with increasing dye concentration was noted, implying reduced adsorption rate due to the progressive occupation of active sites. The Elovich model also fitted the data reasonably well, highlighting the heterogeneous nature of the adsorbent surface and suggesting a multi-stage adsorption process, initial film diffusion, internal particle diffusion, and pore diffusion. The larger α values in comparison to β further indicate that the adsorption process is more favorable than desorption. The IPD model, proposed by Weber and Morris, was used to explore whether intra-particle diffusion controls the rate of adsorption. The qt vs. $t^{0.5}$ plots showed non-zero intercepts and lower R^2 values, indicating that IPD is not the sole rate-limiting mechanism. These findings suggest the presence of multiple diffusion steps, with external and surface interactions playing dominant roles.

In conclusion, the PSO kinetic model best describes the adsorption of TB dye onto the nanoadsorbent of neem bark, supporting the chemisorptive nature of the interaction. While the Elovich model supports surface heterogeneity and diffusion-based mechanisms, the IPD model results confirm that intra-particle diffusion alone does not govern the entire adsorption process [41].

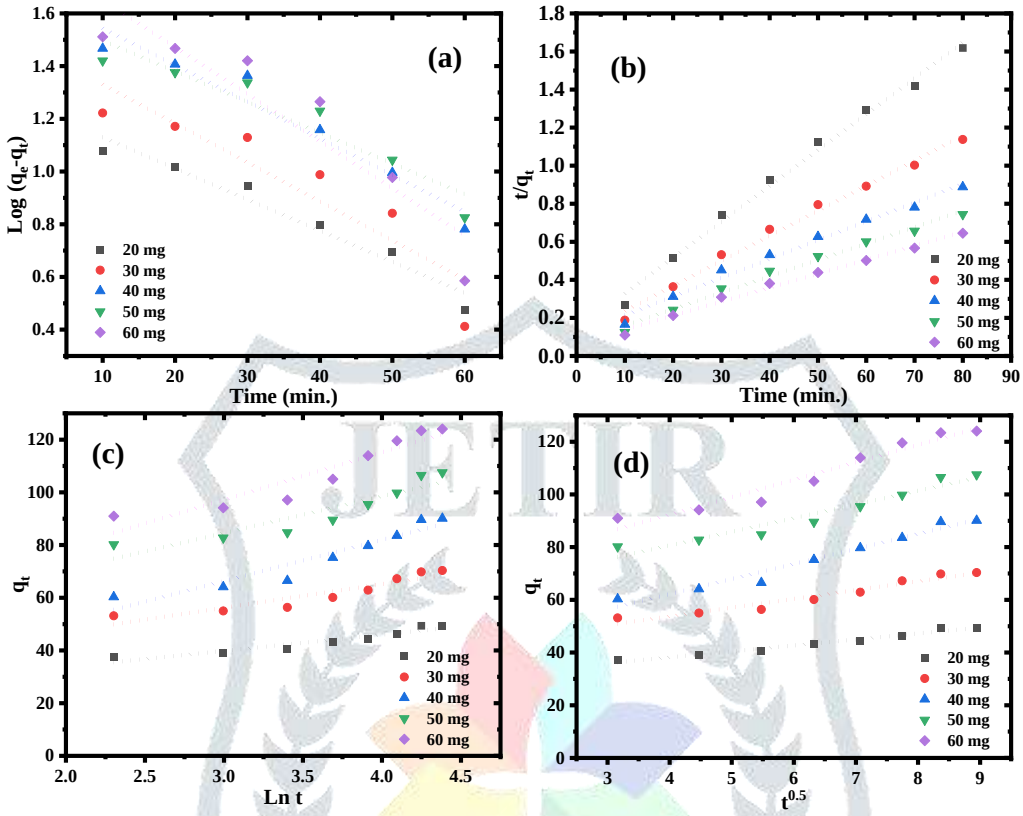

Figure 9: Kinetic models for TB dye adsorption onto activated carbon derived from neem bark nanoadsrbent: (a) Pseudo-first-order, (b) Pseudo-second-order, (c) Elovich model, and (d) Intraparticle diffusion plots.

Table 1: Adsorption Kinetic parameters of TB dye onto nanoadsorbent derived by neem bark

Kinetics Models	Parameters	Dye Concentration				
		20 mg	30 mg	40 mg	50 mg	60 mg
First order	q_e, exp	49.382	69.821	89.631	106.524	123.43
	K_1	0.027	0.034	0.032	0.026	0.041
	q_e, cal	17.725	30.126	48.143	41.051	67.589
	R	0.978	0.916	0.97	0.949	0.928
Second order	q_e, cal	53.05	76.046	101.317	116.144	136.426
	K_2	0.0025	0.00164	0.0008	0.0009	0.0008
	R	0.996	0.995	0.993	0.994	0.996
Elovich	β	0.162	0.111	0.064	0.072	0.055
	α	195.612	230.556	54.282	297.469	197.707
	R	0.952	0.934	0.951	0.921	0.939
Intraparticle	K_{id}	2.258	3.322	5.712	5.185	6.61
	C	29.153	40.437	39.332	59.903	65.918
	R	0.984	0.973	0.982	0.967	0.974

D. Adsorption Isotherm Studies

Isotherm modelling plays a crucial role in understanding the equilibrium distribution of adsorbate molecules between the liquid and solid phases. In this study, the equilibrium data for TB dye adsorption onto activated carbon of neem bark nanosorbent were evaluated using four commonly adopted isotherm models: Langmuir, Freundlich, Temkin, and Dubinin–Radushkevich (D–R). These models were employed to explore the adsorption mechanism and determine the best-fitting model that characterizes the dye–adsorbent interaction. Among the models tested, the Langmuir isotherm showed the strongest correlation with the experimental data, with a high R^2 value of 0.999. This model assumes monolayer adsorption on a homogeneous surface with uniform energy sites

and no adsorbate-adsorbate interactions. The maximum adsorption capacity (q_{max}) was found to be 75.76 mg/g, and the separation factor (R_L) was 0.061, indicating favorable adsorption conditions ($0 < R_L < 1$) [42]. The Freundlich model, which accounts for heterogeneous surface energies and multilayer adsorption, also demonstrated a good fit ($R^2 = 0.9$). The Freundlich constant n was calculated as 5.708 (1/n = 0.174), which falls within the favorable range ($0 < 1/n < 1$), indicating efficient adsorption and slight heterogeneity on the adsorbent surface [43]. The Temkin model, which considers adsorbent–adsorbate interactions and a linear decline in heat of adsorption, provided a moderate correlation ($R^2 = 0.978$). While it also matches the experimental data as well as the Langmuir or Freundlich models, it offers insight into the energetics of the adsorption process [44]. The D–R isotherm, used to differentiate between physical and chemical adsorption mechanisms, produced the lowest R^2 value (0.896), indicating poor conformity. The calculated mean adsorption energy (E) was $3.1x10^3$ kJ/mol, an unusually high value inconsistent with typical physisorption, suggesting that this model does not accurately describe the current adsorption system [45]. In conclusion, the Langmuir model best represents the adsorption behavior of TB on the neem bark activated carbon nanoadsorbent, confirming monolayer adsorption on a uniform surface. The Freundlich model further supports the presence of surface heterogeneity, while the Temkin and D–R models, though less accurate, provide additional understanding of interaction energies and adsorption mechanisms.

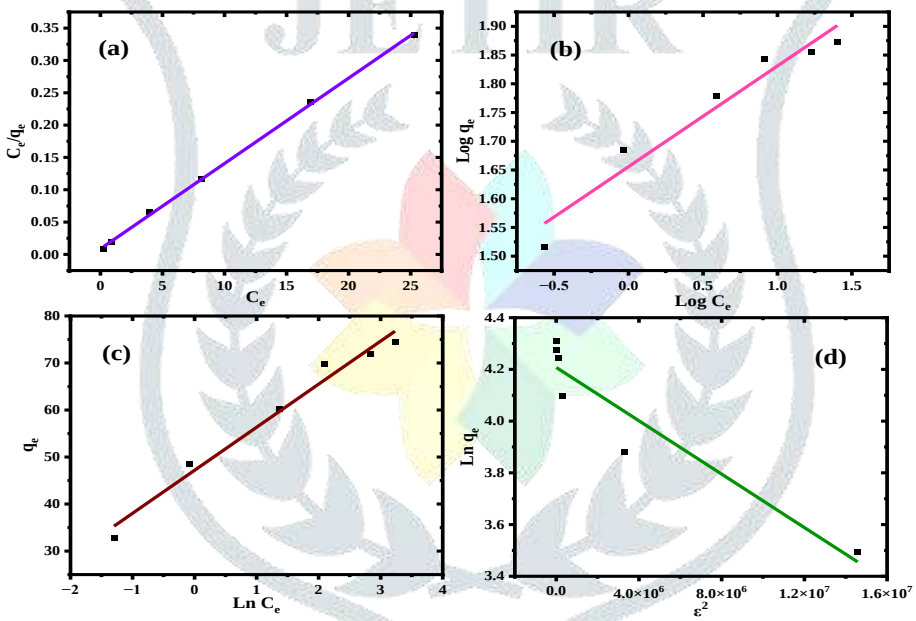

Figure 10: Isotherm model plots for the adsorption of TB dye onto *Azadirachta indica* (neem) bark-derived nanoadsorbent: (a) Langmuir, (b) Freundlich, (c) Temkin, and (d) Dubinin–Radushkevich (D–R) models.

Table 2: Isotherm Model Analysis for the Adsorption of TB Dye onto Azadirachta indica (neem) bark-derived nanoadsorbent.

Isotherms	Paramerers	Values of isotherm parameters
Langmuir	q_{max}	75.76
	b_L	1.53
	R_L	0.061
	R^2	0.999
Freundlich	K_f	45.27
	n	5.708
	R^2	0.945
Tempkin	bT	247.95
	K_T	172.72
	B_T	9.16
	R^2	0.978
D-R	K_{id}	5.16×10^{-8}
	E	3.1×10^3
	R^2	0.896

E. Thermodynamic Analysis of the Adsorption Process

Understanding the thermodynamic behavior of adsorption is essential for assessing the viability and efficiency of dye removal from aqueous systems using nanoadsorbents. Thermodynamic parameters such as Gibbs free energy (ΔG°), enthalpy change (ΔH°), and entropy change (ΔS°) are commonly used to interpret the spontaneity and nature of the adsorption process. A negative ΔG° value suggests that the adsorption occurs spontaneously [46]. A positive ΔS° indicates increased randomness at the solid–liquid interface, implying greater disorder and more favorable adsorption interactions [47]. In contrast, a negative ΔS° signifies a reduction in disorder, pointing to a more structured adsorption process [48].

Table 3: Thermodynamic parameters related to the adsorption of TB dye onto the activated carbon of neem bark nanoadsorbent.

Temperature (K)	ΔG° (kJ mol^{-1})	ΔH° (kJ mol^{-1})	ΔS° (J mol^{-1} K^{-1})
298.15	-11.16		
308.15	-11.98	22.47	112.498
318.15	-13.42		

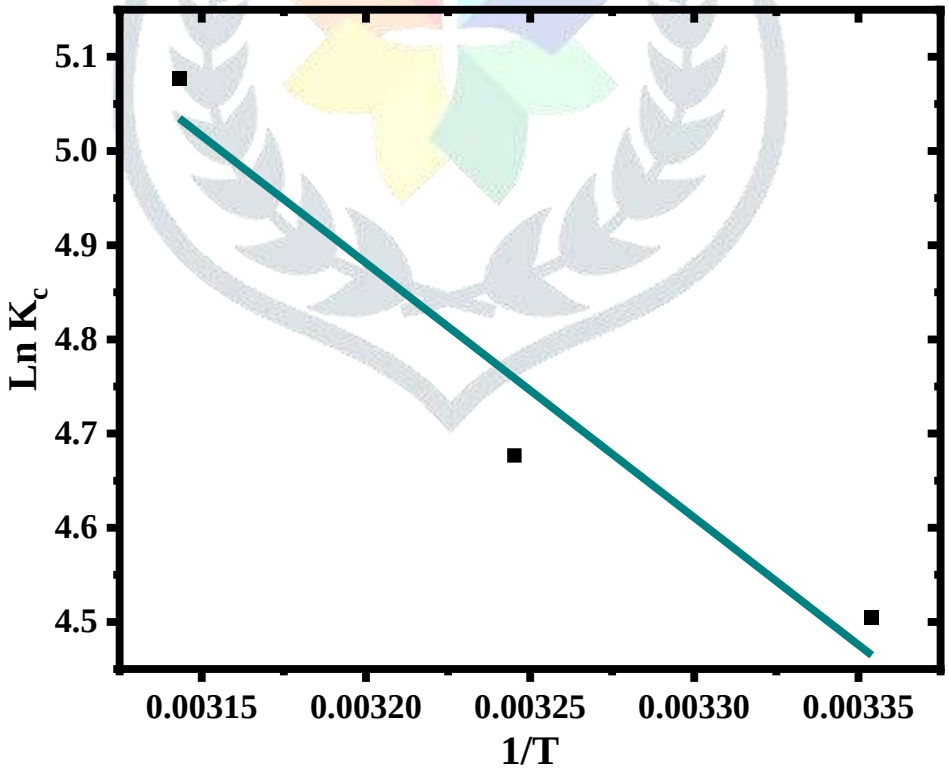

Figure 11: Correlation between temperature and the equilibrium constant (K_c) for the adsorption of TB dye onto *Azadirachta indica* (neem) derived nanoadsorbent.

F. Evaluation of the Regeneration Efficiency

The long-term applicability of an adsorbent for water purification largely depends on its stability and reusability [49]. The recyclability of the synthesized neem bark-derived activated carbon nanoadsorbent was evaluated through four successive adsorption–desorption cycles using TB dye. After each cycle, the spent adsorbent was recovered via centrifugation, thoroughly rinsed with water and ethanol to remove residual dye, and then dried at 85 °C for four hours before reuse. As illustrated in Fig. 14, the removal efficiency remained relatively consistent across cycles. Even after the fourth reuse, the adsorbent retained approximately 90% of its initial TB removal capacity, demonstrating excellent stability and regeneration potential.

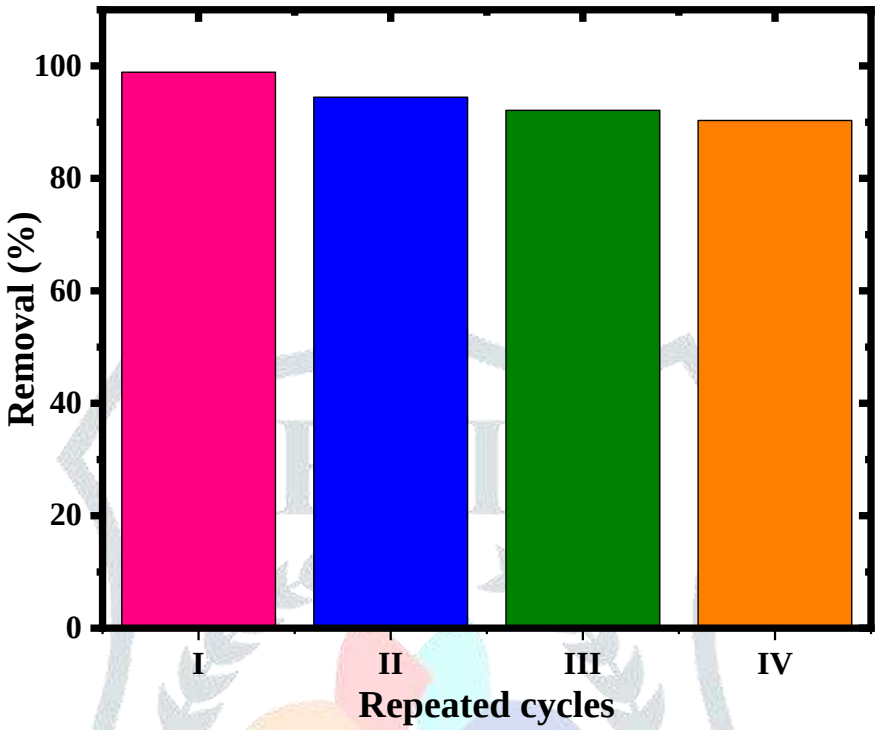

Figure 12: Reusability performance of *Azadirachta indica* (neem) derived nanoadsorbent: Evaluation of Recycling Efficiency Over Multiple Adsorption–Desorption Cycles

IV. Conclusion

The findings of this study demonstrate that the nanoadsorbent synthesized from *Azadirachta indica* (neem) bark is highly effective in removing TB dye from aqueous solutions. A key feature of this adsorbent is the presence of surface functional groups such as hydroxyl (-OH) and carbonyl (-C=O), which facilitate binding with the dye molecules during the adsorption process. Several parameters, including contact time, adsorbent dosage, and initial dye concentration, influenced adsorption efficiency. The nanoadsorbent exhibited a high BET surface area and significant pore volume, with pore formation confirmed through FESEM analysis. HRTEM imaging revealed that the particle size of the nanoadsorbent ranged up to 200 nm. Optimal dye removal occurred at pH 12, with a maximum removal efficiency of 98.33%. The Langmuir isotherm model provided the best fit for the equilibrium data, suggesting monolayer adsorption on a homogeneous surface and indicating strong interaction between the dye and the adsorbent. Additionally, the adsorption kinetics followed the pseudo-second-order (PSO) model with an excellent correlation coefficient (R^2 = 1), signifying chemisorption as the dominant mechanism. Thermodynamic analysis confirmed that the adsorption process was both spontaneous and exothermic.

These results highlight the potential of using low-cost, naturally available biomass such as *Azadirachta indica* (neem) bark for developing efficient nanoadsorbents to treat dye-contaminated industrial wastewater. Future work will focus on extending the application of this nanoadsorbent to the removal of other dyes and pollutants.

Acknowledgment

The authors express their sincere gratitude to the following organizations and institutions for their support and contributions to the research:

MRC (Malaviya National Institute of Technology, Jaipur, India
Department of Chemistry, University of Rajasthan, Jaipur, India

V. References

[1] Mustafa, T. Y., Sen, T. K., Sharmeen, A., and Ang, H. M., 2014. Dye and its removal from aqueous solution by adsorption: A review, Advances in Colloid and Interface Science. 209: 172-184. https://doi.org/10.1016/j.cis.2014.04.002

[2] Chung, K., 2016. Azo dyes and human health: a review. J Environ Sci Health C Environ Carcinog Ecotoxicol Rev. 34 (4): 233-261.

[3] Azam, P., Olya, M. E., 2017. Removal of dye from industrial wastewater with an emphasis on improving economic efficiency and degradation mechanism. Journal of Saudi Chemical Society. 21(1): S179-S186. https://doi.org/10.1016/j.jscs.2013.12.008

[4] Mordhiya, B., Sharma, R., Meena, P. L., Meena, P., Selwal, C., 2024. Development of novel adsorbent for removal of organic contaminants from polluted water: kinetic, isotherm, and thermodynamic studies. J IRAN CHEM SOC 21, 835–851 (2024). https://doi.org/10.1007/s13738-023-02964-x

[5] Mordhiya, B., Daga, K., Chandra, S., Aggrawal, S., 2012. Adsorptive Treatment of Methylene Blue Dye from Aqueous Solution Using Moringa Oleifera as an Adsorbent, Nat. Env. & Pll. Tech. 11 (1): 113-116.

[6] Yadav, A., Bagotia, N., Yadav, S., Sharma, A. K., Kumar, S., 2021. Adsorptive studies on the removal of dyes from single and binary systems using Saccharum munja plant-based novel functionalized CNT composites, Environ Technol Innov 24:102015. https:// doi.org/ 10. 1016/j. eti. 2021. 102015

[7] Meena, P. L., Saini, J. K., Surela, A.K., Mordhiya, B., Meena, K.S., and Chhachhia, L.K. 2023. Fabrication of polyaniline-supported MnO_2 nanocomposite for removal of water pollutant: kinetic and isotherm studies. Chem. Sel. 8, e202300724. https://doi.org/10.1002/slct.202300724

[8] Kandisa, R. V., Narayana Saibaba, K.V., Shaik, K. B., and Gopinath R., 2016. Dye Removal by Adsorption: A Review, Journal of Bioremediation & Biodegradation: 07(06), 371. http://doi.org/10.4172/2155-6199.1000371

[9] Kuyucu, A. E., Selçuk, A., Önal, Y. Alacabey, I., Erol, K., 2025. Effective removal of dyes from aqueous systems by waste-derived carbon adsorbent: physicochemical characterization and adsorption studies, Sci Rep. 15: 28835. https://doi.org/10.1038/s41598-025-13685-x

[10] Shi, Y., Baker, J., Feng., C., Wang, X., Li., Z., 2022. Removal of toluidine blue from water using 1:1 layered clay minerals, Advanced Power Technology. 33 (6): 103608. https://doi.org/10.1016/j.apt.2022.103608

[11] Rout, D. R., Jena, H. M., 2021. Removal of malachite green dye from aqueous solution using reduced graphene oxide as an adsorbent, Materialstoday: Proceedings. 47 (5): 1173-1182. https://doi.org/10.1016/j.matpr.2021.03.406

[12] Chakraborty, S., Chowdhury, S., Saha, P. D., 2011. Adsorption of Crystal Violet from aqueous solution onto NaOH-modified rice husk, Carbohydrate Polymers. 86 (4): 1533-1541. https://doi.org/10.1016/j.carbpol.2011.06.058

[13] Azzaz, A. A., Jellali, S., Hamed, N. B. H., Jery, A. E., Khezami, L., Assadi, A. A., and Amrane, A., 2021. Photocatalytic Treatment of Wastewater Containing Simultaneous Organic and Inorganic Pollution: Competition and Operating Parameters Effects, Catalysts. 11 (7): 855. https://doi.org/10.3390/catal11070855

[14] Foroutan, R., Peighambardoust, S. J., Peighambardoust, S. H., Pateiro, M., and Lorenzo, J. M., 2021. Adsorption of crystal violet dye using activated carbon of lemon wood and activated carbon/Fe3O4 magnetic nanocomposite from aqueous solutions: a kinetic, equilibrium and thermodynamic study. Molecules, 26(8), 2241. https://doi.org/10.3390/molecules26082241

[15] Garud, H. B., Patil, P. H., Jadhav, S. A., Patil, P. S., Kalantre, V. A., Burungale, S. H., 2025. Effective removal of dyes from their mixture in solution by waste-derived microadsorbents: Physicochemical characterization and adsorption removal studies, Next Research. 2 (2): 100235. https://doi.org/10.1016/j.nexres.2025.100235

[16] Dutta, S., Gupta, B., Srivastva, S. K., Gupta, A. K., 2021. Recent advances on the removal of dyes from wastewater using various adsorbents: a critical review, Mater. Adv. 2: 4497-4531. https://doi.org/10.1039/D1MA00354B

[17] Saidulu, D., Gupta, B., Gupta, A. K., Ghosal, P. S., 2021. A review on occurrences, eco-toxic effects, and remediation of emerging contaminants from wastewater: Special emphasis on biological treatment based hybrid systems, Journal of Environmental Chemical Engineering. 9 (4): 105282. https://doi.org/10.1016/j.jece.2021.105282

[18] Zhou, L., Zhou, H., Hu, Y., Yan, S., Yang, J., 2019. Adsorption removal of cationic dyes from aqueous solutions using ceramic adsorbents prepared from industrial waste coal gangue, Journal of Environmental Management. 234: 245-252. https://doi.org/10.1016/j.jenvman.2019.01.009

[19] Santos, Silvia C. R., Boaventura, R. A. R., 2008. Adsorption modelling of textile dyes by sepiolite, Applied Clay Science. 42(1-2): 137-145. https://doi.org/10.1016/j.clay.2008.01.002

[20] Luo, P., Zhao, Y., Zhang, B., Liu, J., Yang, Y., Liu, J., 2010. Study on the adsorption of Neutral Red from aqueous solution onto halloysite nanotubes, Water Research. 44: 1489-1497. https://doi.org/10.1016/j.watres.2009.10.042

[21] Faria, P. C. C., Órfão, J. J. M., Pereira, M. F. R., 2004. Adsorption of anionic and cationic dyes on activated carbons with different surface chemistries, Water Research, 38: 2043-2052. https://doi.org/10.1016/j.watres.2004.01.034

[22] Selvam, P. P., Preethi, S., Basakaralingam, P., Thinakaran, N., Sivasamy, A., Sivanesan, S., 2008. Removal of rhodamine B from aqueous solution by adsorption onto sodium montmorillonite, Journal of Hazardous Materials. 155 (1-2): 39-44. https://doi.org/10.1016/j.jhazmat.2007.11.025

[23] Alpat, S.K., Özbayrak, O., Alpat, S., Akçay, H., 2008. The adsorption kinetics and removal of cationic dye, Toluidine Blue O, from aqueous solution with Turkish zeolite, Journal of Hazardous Materials. 151 (1), 213-220. https://doi.org/10.1016/j.jhazmat.2007.05.071

[24] Jangra, A., Kumar, R., Singh, D., Kumar, H., Kumar, J., Kumar, P., Kumar, S., 2024. Remediation of toluidine blue O dye from aqueous solution using surface functionalized magnetite nanoparticles, Water Practice and Technology. 19 (4): 1119–1134. https://doi.org/10.2166/wpt.2024.063

[25] Patel, H., Vashi, R. T., 2010. A study on removal of Toluidine blue dye from aqueous solution by adsorption onto Neem leaf powder, World Academy of Science Engineering and Technology. 70: 831-836.

[26] Yonan, E. N., Sher Mohammed, N. M., Qasim, A. K., 2024. Green synthesis and characterisation of monometallic (Ni) and bimetallic (Ni-Ag) nanoparticles using Cicer Arietinum leaf extract and their applications for adsorption of toluidine blue. International Journal of Environmental Analytical Chemistry 2024, 104 (17), 5264-5279. https://doi.org/10.1080/03067319.2022.2118594

[27] Brandão, W. Q., Maciel, B. G., Lima, E. M. A., Mojica-Sánchez, L. C., Da Silva, R. J., De Melo, C. P., 2023. Carboxymethylcellulose magnetic composite for adsorptive removal of cationic toluidine blue dye, Materials Chemistry and Physics. 303, 127782. https://doi.org/10.1016/j.matchemphys.2023.127782

[28] Ofudje, E. A., Sodiya, E. F., Akinwunmi, F., Ogundiran, A. A., Oladeji, O. B., Osideko. O. A., 2022. Eggshell derived calcium oxide nanoparticles for Toluidine blue removal, Desalination and Water Treatment. 247: 294-308. https://doi.org/10.5004/dwt.2022.28079

[29] Asheghhosseini, A., Zolgharnein, J., 2020. Iron terephthalate metal–organic framework (MOF-235) as an efficient adsorbent for removal of toluidine blue dye from aqueous solution using Box–Behnken design as multivariate optimization approach, Journal of the Iranian Chemical Society. 17 (10): 2663-2673. https://doi.org/10.1007/s13738-020-01958-3

[30] Bretanha, M. S., Dotto, G. L., Vaghetti, J. C. P., Dias, S. L. P., Lima, E. C., Pavan, F. A., 2016. Giombo persimmon seed (GPS) an alternative adsorbent for the removal Toluidine Blue dye from aqueous solutions, Desalination and Water Treatment. 57 (58): 28474-28485. https://doi.org/10.1080/19443994.2016.1179223

[31] Bharathi, K. S., and Ramesh, S. T., 2013. Removal of dyes using agricultural waste as low-cost adsorbents: a review, Appl Water Sci. 3:773–790. http://doi.org/10.1007/s13201-013-0117-y

[32] Kadhom, M., Albayati, N., Alalwan, H., Al-Furaiji, M., 2020. Removal of dyes by agricultural waste, Sustainable Chemistry and Pharmacy. 16: 100259. https://doi.org/10.1016/j.scp.2020.100259

[33] Khan, E. A., Shahjahan, Khan, T. A., 2018. Adsorption of methyl red on activated carbon derived from custard apple (Annona squamosa) fruit shell: Equilibrium isotherm and kinetic studies, Journal of Molecular Liquids. 249: 1195-1211. https://doi.org/10.1016/j.molliq.2017.11.125

[34] Malik, D. S., Jain, C. K., Yadav, A. K., 2015. Preparation and characterization of plant-based low-cost adsorbents, Journal of Global Biosciences. 4 (1): 1824-1829.

[35] Jain, R., Gupta, V. K., Sikarwar, S., 2010. Adsorption and desorption studies on hazardous dye Naphthol Yellow S, J Hazard Mater. 182 (1-3): 749-756. http://doi.org/ 10.1016/j.jhazmat.2010.06.098.

[36] Gupta, V. K., Saleh, T. A., 2013.Sorption of pollutants by porous carbon, carbon nanotubes and fullerene- an overview, Environ Sci Pollut Res Int. 20(5):2828-43. http://doi.org/10.1007/s11356-013-1524-1.

[37] Sahoo, J.K., Sukla, R.K., Pradhan, A., Sahoo, S.K., Rath, J., 2024. Removal of Eriochrome Black T dye using Plant Based Bio-Adsorbent: A Review, Letters in Applied NanoBioScience. 13 (2):73. https://doi.org/10.33263/LIANBS132.073

[38] Honarmand, M., Golmohammadi, M., Naeimi, A., 2019. Biosynthesis of tin oxide (SnO_2) nanoparticles using jujube fruit for photocatalytic degradation of organic dyes. Adv. Powder Technol. 30 (8):1551–1557. https://doi.org/10.1016/j.apt.2019.04.033.

[39] Aziz, E.K., Abdelmajid, R., Rachid, L.M., Mohammadine, E.H., 2018. Adsorptive removal of anionic dye from aqueous solutions using powdered and calcined vegetables wastes as low-cost adsorbent. Arab J. Basic Appl. Sci. 25: 93–102, https://doi.org/10.1080/25765299.2018.1sa517861.

[40] Nazir, R., Khan, M., Rehman, R.U., Shujah, S., Khan, M., Ullah, M., Zada, A., Mahmood, N., Ahmad, I., 2020. Adsorption of selected azo dyes from an aqueous solution by activated carbon derived from Monotheca buxifolia waste seeds. CAAS Agricultural Journ. 15: 166–172, https://doi.org/10.17221/59/2019-SWR

[41] Hasanzadeh, M., Simchi, A., Far, H. S., 2019. Kinetics and adsorptive study of organic dye removal using water-stable nanoscale metal organic frameworks, Materials Chemistry and Physics. 233: 267-275. https://doi.org/10.1016/j.matchemphys.2019.05.050

[42] Irwan, M., Nadir, M., Patmawati Y., 2023. Isotherm and Kinetic Study of Dyes Solution, International Journal of Multidisciplinary Research and Publications. 6 (6): 1-4.

[43] Gimbert, F., Morin-Crini, N., Renault, F., Badot, P. M., Crini, G., 2008. Adsorption isotherm models for dye removal by cationized starch-based material in a single component system: Error analysis, Journal of Hazardous Materials. 157 (1): 34-46. https://doi.org/10.1016/j.jhazmat.2007.12.072

[44] Ravansalar, S., Zolgharnein, J., and Dermanaki Farahani, S. A., 2025. Facile Synthesis of Ag@CaO@$CoFe_2O_4$ Magnetic Nanocomposite as a Highly Efficient Adsorbent for Remediation of Toluidine Blue from Water Sources and Experimental Design Optimization, Water Air Soil Pollut. 236: 573. https://doi.org/10.1007/s11270-025-08212-7

[45] Murphy, O. P., Vashishtha, M., Palanisamy, P., Kumar, K. V., 2023. A Review on the Adsorption Isotherms and Design Calculations for the Optimization of Adsorbent Mass and Contact Time, ACS Omega. 8: 17407-17430.

[46] Handayani, T., Emriadi, Deswati, Ramadhani, P., Zein, R., 2024. Modelling studies of methylene blue dye removal using activated corn husk waste: Isotherm, kinetic and thermodynamic evaluation, South African Journal of Chemical Engineering. 47: 15-27. https://doi.org/10.1016/j.sajce.2023.10.003

[47] Agarwal, S., Jain, H., Dhupper, R., Mathur, A., 2025. Optimizing Methyl Orange Dye Removal from Aqueous Solutions Using White Chrysanthemum Floral Waste-Derived Bioadsorbent: A Study of Kinetics, Thermodynamics, Isotherms, and RSM Optimization, Int J Environ Res. 19: 104. https://doi.org/10.1007/s41742-025-00773-z

[48] Xu, W., Chen, Y., Zhang, W., and Li, B., 2019. Fabrication of graphene oxide/bentonite composites with excellent adsorption performances for toluidine blue removal from aqueous solution. Advanced Powder Technology, 30(3): 493–501.

[49] Siddiqui, M. R. H., Adil, S., Assal, M., Ali, R., & Al-Warthan, A. (2013). Synthesis and characterization of silver oxide and silver chloride nanoparticles with high thermal stability. Asian Journal of Chemistry, 25(6), 3405–3409.